Estimation of Geoacoustic Properties of Marine Sediment Using a Hybrid Differential Evolution Inversion Method

Yong-Min Jiang, *Member, IEEE*, N. Ross Chapman, *Fellow, IEEE*, and Peter Gerstoft

Abstract—This paper reports the inversion of midfrequency (1500–4500 Hz) chirps from a short-range transmission experiment conducted on the New Jersey Continental Shelf during the 2006 Shallow Water Experiment (SW06). The source was held at different depths and the sound signals were recorded at a vertical line array to investigate the interactions with the sea bottom at various grazing angles. Strong reflections from the sediment layer were seen in the data for all of the sources. Due to the presence of complex microstructures in the thermocline of the oceanic sound-speed profile, fluctuations both in amplitude and arrival time of the direct path arrivals were observed. Time variation of the water-column environment was also evident during the source transmissions. To mitigate the effects of the ocean environment on the seabed property estimation, a multistage optimization inversion was employed. The sound speed and the experimental geometry were inverted first using only the travel times of the water-column arrivals. The bottom sound speed and the sediment layer thickness were then inverted by matching the travel times of the bottom and sub-bottom reflections. The average of the estimated values for the sediment sound speed is 1598 m/s, consistent with *in situ* measurements from other experiments in the vicinity.

Index Terms—Differential evolution (DE), downhill simplex (DHS), empirical orthogonal function (EOF), geoacoustic inversion, hybrid optimization algorithm, sediment property, travel-time inversion.

I. INTRODUCTION

SOUND propagation in the littoral regions is strongly influenced by the marine sediment properties. It is also affected by the water column environment where the sound-speed profile (SSP) varies temporally and spatially due to internal waves, fronts, eddies, diurnal tides, etc. The influence of ocean environmental variation on the sound propagation at high frequencies is more severe, since the sensitivity of the signal to the oceanic environment variation increases with increasing signal frequency. This fact clearly brings more challenges to the estimation of marine sediment properties in the shallow-water environment.

Y.-M. Jiang and N. R. Chapman are with the School of Earth and Ocean Sciences, University of Victoria, Victoria, BC V8W 3V6 Canada (e-mail: minj@uvic.ca; chapman@uvic.ca).
P. Gerstoft is with the Marine Physical Laboratory, Scripps Institution of Oceanography, La Jolla, CA 92093-0238 USA (e-mail: gerstoft@ucsd.edu).

In summer 2006, a U.S. Office of Naval Research sponsored, multidisciplinary, multi-institution, and multinational Shallow Water Experiment (SW06) was carried out at sites near the shelf break on the New Jersey continental shelf [1]. A central objective of the geoacoustic component of SW06 was to characterize the ocean bottom in a complex oceanic environment within the frequency band from 50 to 20 000 Hz. In this paper, we present the inversion results of midfrequency (MF) (1500–4500 Hz) sound transmissions collected at one of the vertical line arrays (VLAs). During the experiment, the source was held at different depths at a range of 230 m from the VLA. This experimental geometry provides wide-angle grazing angle coverage, similar to the fixed receiver and towed source geometry described by Holland and Osler [2]. To account for the variable water column SSP, the effective oceanic SSP for each source depth was inverted before the sea bottom properties were inverted. The inversions of the water-column SSP, sediment sound speed, and thickness were carried out by use of a hybrid optimization algorithm: adaptive simplex differential evolution (ASDE).

The remainder of this paper is organized as follows. Section II briefly describes the experiment and the environmental and acoustic observations. Section III introduces the ASDE inversion method. Section IV presents the inversion of the experimental data. Section V summarizes the work.

II. DESCRIPTION OF THE EXPERIMENT

A. Experimental Site and Geometry

The experiment was carried out on JD243 (Julian Day 243, i.e., August 31, 2006) near the shelf break of New Jersey Continental Shelf. The data analyzed here were recorded on a VLA developed by Marine Physical Laboratory (MPL-VLA1) at (39° 1.4771′ N, 73° 2.259′ W). MPL-VLA1 was in the center of a 1-km^2 area that was selected for low-frequency and MF acoustic experimental studies. The vicinity of the experimental site was extensively surveyed previously, and also during SW06. The site is located on the low-speed clay outershelf sediment wedge [3]. A distinguishing feature of the ocean bottom at the SW06 site is a ubiquitous subsurface seismic "R" reflector. There is also an erosional channel above the "R"-reflector in some of the area [3]–[5]. If a sound speed of 1600 m/s is used as the reference speed, the depth of the "R"-reflector is ∼20 m and the erosional channel is ∼14 m under the seafloor between the source and MPL-VLA1[1] [6].

---

[1]The chirp seismic reflection data along the source and MPL-VLA1 was provided by Dr. J. A. Goff.
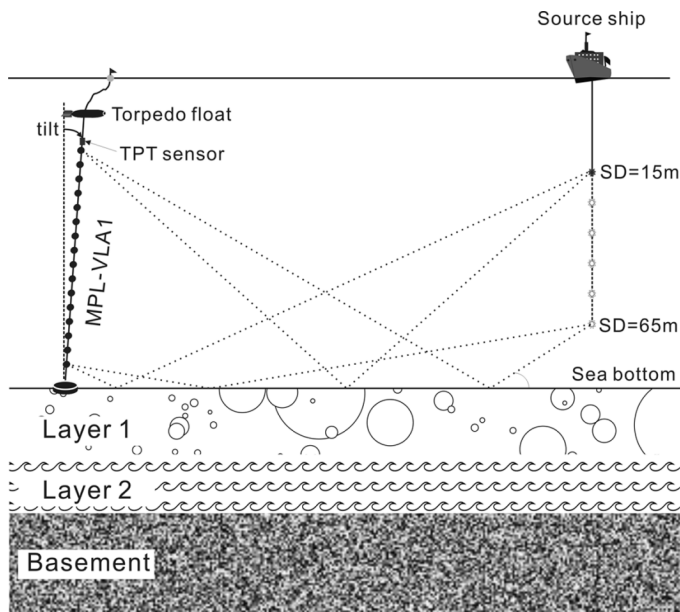
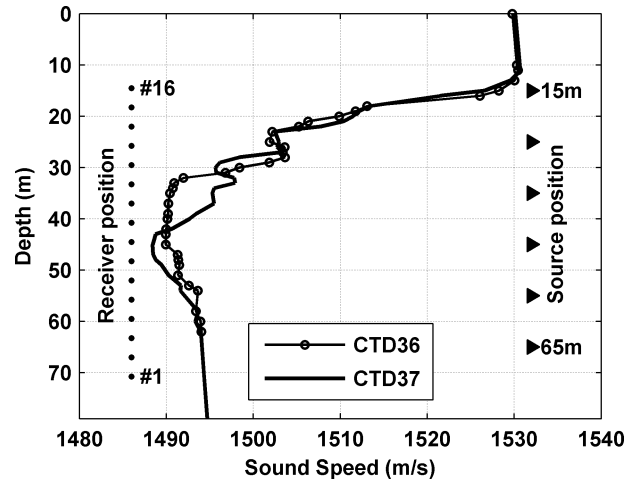Fig. 1.   Experimental geometry and geoacoustic model.

Fig. 2.   CTD casts made at source position before and after the experiment.
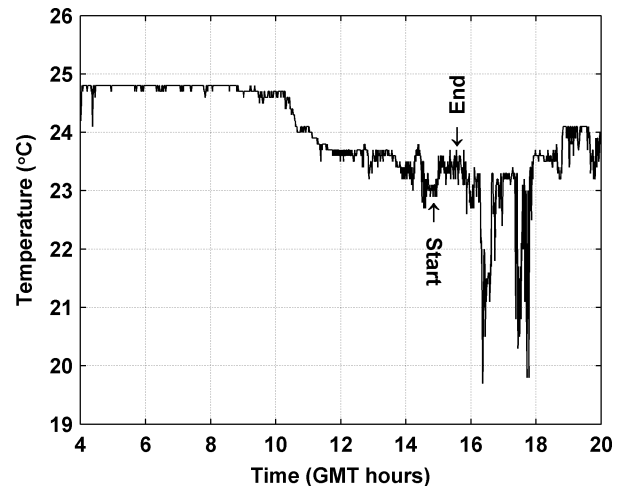

Fig. 3.   Temperature measured by TPT sensor on MPL-VLA1 on JD243. The sample rate of the temperature is 1 sample per 30 s.

There were 16 hydrophones evenly spaced at 3.75 m on MPL-VLA1, with the bottom hydrophone at 8.2 m above the seafloor. During the experiment, the source was lowered from the source ship into the water column and held for 5 min at depths of 15–65 m in 10-m intervals. The source ship held position at 230 m from MPL-VLA1 using a dynamic positioning system (DPS). The bathymetry between the source and the VLA was nearly flat with the water depth around 79 m at the VLA and 79.6 m at the source. A tilt/pressure/temperature (TPT) sensor located 0.5 m above the top hydrophone monitored the tilt of the VLA and the water temperature variations. The nominal depth of the TPT sensor was 14.05 m. During the experiment, the torpedo float attached to the top of the VLA was driven by the winds and currents so that the VLA leaned to a specific direction. The TPT sensor showed that the VLA tilt was $2° \pm 0.6°$ during the MF source lowering experiment.

Fig. 1 depicts the experimental geometry and the geoacoustic model for the data analysis. The experimental geometry ensures wide grazing angle coverage of the seafloor reflection by altering the source depth in the water. The data analyzed here were collected within a 45-min period.

B. Ocean Environment Observations

Two conductivity–temperature–depth (CTD) profiles were measured at the source position for this experiment. CTD36 was recorded at 14:27:00 GMT (Greenwich Mean Time, all the times hereafter are GMT), the beginning of the source lowering event. CTD37 was measured at 15:12:00, which was the end time of the event. Fig. 2 shows the SSPs derived from those two CTD casts. Notable differences between the two SSPs are found between depths of 20 and 60 m. Both SSPs have microstructures in the thermocline depths.

The temperature at the TPT sensor on the VLA on JD243 is plotted in Fig. 3. It is evident that the temperature was stable until 08:40:00. Large temperature fluctuations are found between 16:00:00 and 18:00:00. A notable temperature difference

is seen between the start and end times of the experiment, and there are observable temperature fluctuations. The temperature fluctuation observed at the VLA indicates that the variations of the CTD casts in Fig. 2 are caused by the possible oceanic activities.

C. Acoustic Data

MF chirps (LFM signals) swept from 1.5 to 4.5 kHz over 1-s duration were repeated every second. The signals received at the 16 hydrophones on the VLA were compressed by matched-filter processing. Fig. 4 shows the envelopes of the compressed signals in a logarithmic scale. In the preliminary stage of the data analysis, the ray tracing code BELLHOP [7] was employed to identify the arrivals such as the direct, surface-reflected (SR), bottom-reflected (BR), surface-reflected–bottom-reflected (SRBR), and bottom-reflected–surface-reflected (BRSR) paths. Several observations are made from the matched-filtered signals.

1) Large amplitude fluctuations of the direct and SR paths are evident for all the source depths. The signal amplitude fluctuations for the 15–45-m sources are larger than the
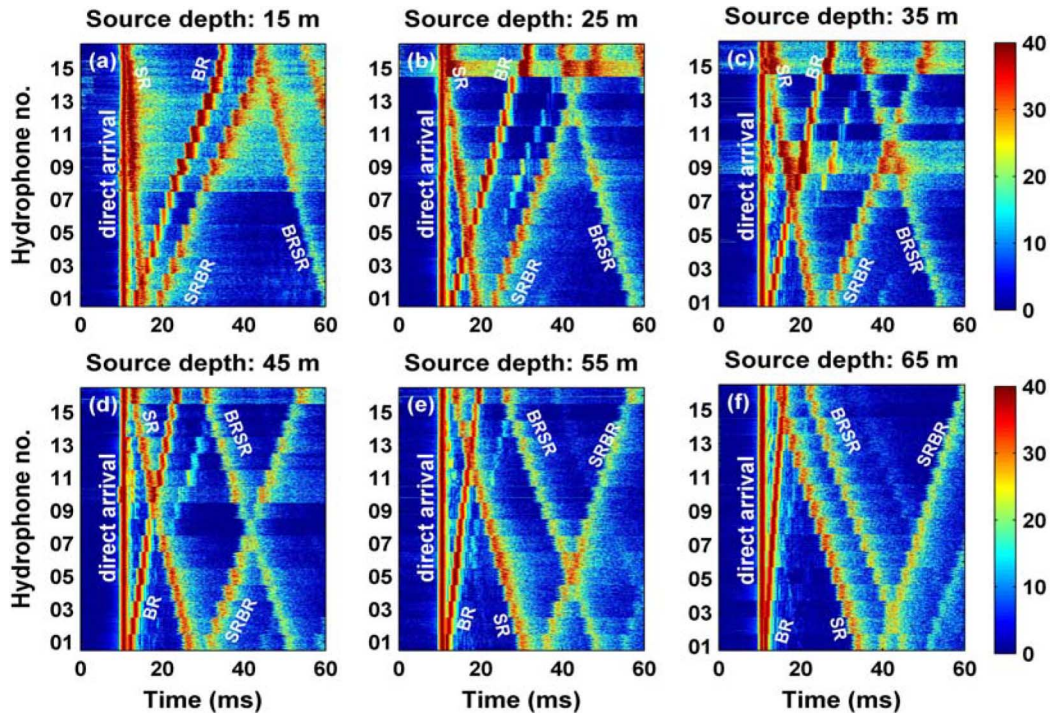
Fig. 4. Matched-filtered chirp signals measured at 16 hydrophones on MPL-VLA1 for six source depths. In each panel, the signals were normalized by the maximum value of the signals from 16 hydrophones, and then plotted in the logarithmic scale. Transmissions within 1 min were stacked vertically to generate one hydrophone's signal, and then the signals from all of the hydrophones were stacked to represent the received signals for one source depth transmission. Color bar units: decibels.

ones for the 55–65-m sources. The amplitude fluctuations of the BR paths are relatively small.

2) The arrival time of the direct path is used to align the traces. Large arrival time fluctuation of the SR path is observed; see the SR signals for the hydrophones 8–15 in Fig. 4(a), for example. The arrival time fluctuation of the BR path is generally weaker.

3) Broadened direct arrivals in the signal duration are observed in the source–receiver pairs separated by the thermocline.

4) At least one reflection from a sub-bottom layer is seen for the 25–65-m source depths, i.e., the arrivals between the BR and SRBR paths for the 25- and 35-m sources, the BR and BRSR paths for the 45-m source, the BR and SR/BRSR paths for the 55-m source, and the BR and SR paths for the 65-m source. Arrivals are also identified immediately after the BR paths at the hydrophones 8–14 for the 15-m source, likely indicating a layer that is close to the sea bottom. These signals were not used in the inversion because of the limited time resolution of the signal.

III. INVERSION APPROACH

A. The Impact of the Water-Column SSP on the Received Signals

A BELLHOP simulation was carried out to investigate the signal amplitude fluctuation of the direct path. Fig. 5 displays the ray tracing result for the source–receiver pair at the nominal depths of 45/18.5 m. The SSP used in this simulation is derived from CTD36. Multiple direct paths are seen in Fig. 5. It is easy
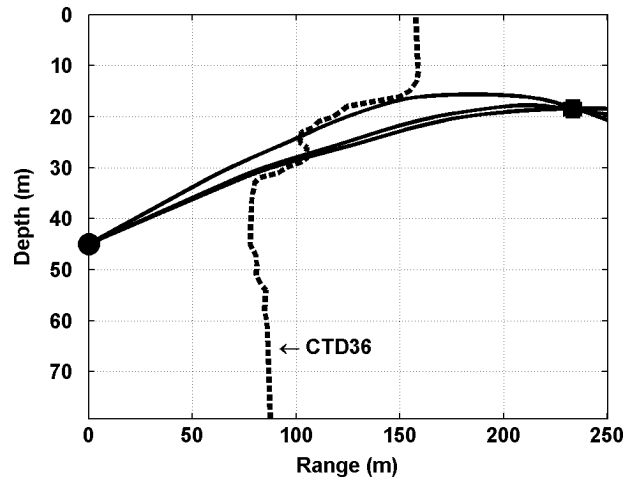

Fig. 5. Multiple direct paths due to the microstructures in the water-column SSP. The source position is represented by the circle and the receiver position is represented by the square.

to conclude that the broadened direct arrival is a result of the interference of the multiple direct paths.

BELLHOP was also used to predict the travel times of the direct, SR, BR SRBR, and BRSR arrivals for all the source depths. Both SSPs derived from CTD36 and CTD37 are used in the simulation. Fig. 6 shows the direct, SR, and BR path predictions for the 25-m source. The experimental geometry was set to nominal values: 79.0-m water depth, 230-m source–receiver range, and no array tilt. Fig. 6 shows that the travel-time predictions using CTD36 and CTD37 are different. The differences
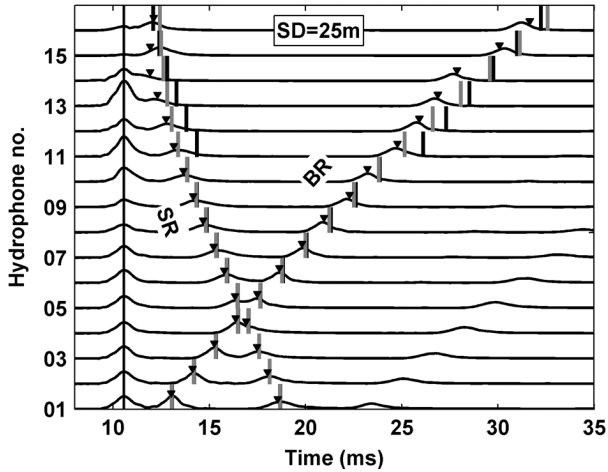
Fig. 6. Travel-time predictions for the 25-m source using CTD36 (short black vertical lines) and CTD 37 (short gray vertical lines). The travel-time signals (horizontal curves) are obtained by averaging the signals over 1 min for each hydrophone. The black triangles indicate the travel-time prediction using the inverted SSP.

between the measured and modeled travel times are also notable. Considering the time resolution of the transmitted signal, which is approximately the inverse of the signal bandwidth, the travel-time errors between the measured and modeled data are not negligible. These travel-time errors might be caused by incorrect information of either the experimental geometry or the water-column SSP. The differences between the two predictions shown in the figure are due to the different SSPs, since the experimental geometry for both cases is kept the same.

B. Inversion Strategy

We may conclude from Section III-A that the water-column SSP has considerable impact on the received signals. The approach of generating a reflection coefficient versus grazing angle curve is not effective for an inversion because of the strong amplitude fluctuation of the direct arrivals, although the experimental geometry is capable of providing wide angular coverage of the bottom reflection. Inversions that involve amplitude information of the direct path are not considered for the same reason. Instead, travel-time information is used in this study. As a result, only sediment sound speed and layer thickness can be inverted since travel time is not sensitive to the sediment density and attenuation.

A multiple stage inversion was carried out as follows.

1) Invert for the experimental geometry including water depth (WD), range (R), source depth (SD), and array tilt. Only the direct, SR, and BR paths in the water are used at this stage since the travel times of the water column paths are not sensitive to the sub-bottom properties. We have the option to choose either the data from the 15-m source or the 65-m source, since CTD36 was measured just before the 15-m transmission and CDT37 was taken immediately after the 65-m transmission. Because the SR path fluctuation is relatively larger for the 15-m source, CDT37 and the data from the 65-m transmission are used to determine the experimental geometry. At this stage, the water-column SSP is assumed known.

2) Invert for the water-column SSP, SD, and the VLA tilt for the 25–55-m sources. At this stage, WD and R are replaced by the inverted values from the previous step. The inversions also use the travel-time information of water-column-only paths such as the direct, SR, and BR arrivals.

3) Invert for the sediment sound speed and layer thickness. At this stage, the ocean SSP and the experimental geometry are fixed at the inverted values from the previous steps. The BR and sub-bottom reflections are used in the inversions.

C. The Objective Function

The objective function for the travel-time inversion is based on comparing the differences of the measured ray travel times $t_{l,n}$, with the modeled ray travel times $T_{l,n}(\mathbf{m})$ generated by an acoustic propagation model for an M-dimensional vector of proposed model parameters $\mathbf{m}$

$$E(\mathbf{m}) = \sum_{l=1}^{N_L} \left\{ \frac{1}{N_{HL}} \sum_{n=1}^{N_{HL}} [t_{l,n} - T_{l,n}(\mathbf{m})]^2 \right\} \qquad (1)$$

where N_L represents the number of layers and N_{HL} is the number of hydrophones used for layer N_L in the inversion. The number of the hydrophones N_{HL} is not necessarily the same for each layer. Note that the travel times used are the relative travel times between specific ray paths and the reference ray paths. For example, in the inversions that use water-column-only ray paths, the reference path is a direct arrival, $N_L = 2$, and N_{HL} equals 16. $t_{l,n}$ and $T_{l,n}(\mathbf{m})$ are the travel-time differences between the BR paths and the direct paths, and the travel-time differences between the SR paths and the direct paths at the nth hydrophones. When inverting for the sediment properties, the reference path is the BR path, and N_L is the number of the sub-bottom layers to be inverted. $t_{l,n}$ and $T_{l,n}(\mathbf{m})$ are the travel-time differences between the sub-bottom paths and the BR paths at N_{HL} hydrophones that contained sub-bottom reflections. The objective function takes any positive value, with 0 indicting a perfect match.

D. The Search Algorithm

A hybrid optimization algorithm ASDE was developed for this study. ASDE embeds the local search algorithm downhill simplex (DHS) into the global search algorithm differential evolution (DE) to retain the advantages of both algorithms and consequently improve the search efficiency.

1) Differential Evolution: DE is a global search algorithm developed by Storn and Price [8], and its use for geoacoustic inversion was described by Snellen *et al.* [9], [10]. It is a population-based evolution algorithm that can be applied to both linear and nonlinear real-valued multimodal objective functions. The main three operations in DE are mutation, crossover, and evaluation operations. The algorithm starts with a random generated N_p population, M-dimensional model parameter vectors as the initial generation

$$\mathbf{m}_i^G, \qquad i = 1, 2, \ldots, N_p \qquad (2)$$

where G represents generation. In the mutation operation, the new perturbed model vectors $\hat{\mathbf{m}}_k^{G+1}$ are generated by adding the weighted difference of two randomly chosen model vectors

$\mathbf{m}_p^G$ and $\mathbf{m}_n^G$ to the third randomly chosen model vectors $\mathbf{m}_k^G$ (see [8] for more mutation strategies)

$$\hat{\mathbf{m}}_k^{G+1} = \mathbf{m}_k^G + \eta \left(\mathbf{m}_p^G - \mathbf{m}_n^G \right) \tag{3}$$

where the weighting factor η is a random number drawn uniformly from $(0, 1]$, and $k, p, n \in [1, N_p]$.

In the crossover operation, the new generation model vectors (offsprings) are generated by choosing the model parameters (genes) to exchange between the perturbed $\hat{\mathbf{m}}_k^{G+1}$ and the original $\mathbf{m}_k^G$ model vector. The jth model parameter of $\mathbf{m}_k^G$ and $\hat{\mathbf{m}}_k^{G+1}$ will be swapped with probability C_R (crossover factor). This procedure is applied to every element in the model vector for each pair of $\mathbf{m}_k^G$ and $\hat{\mathbf{m}}_k^{G+1}$.

A one-on-one competition is performed in the evaluation operation by comparing the energy $E(\mathbf{m})$ (misfit) generated by $\mathbf{m}_k^G$ and $\hat{\mathbf{m}}_k^{G+1}$. The model vector that generates the lower misfit will be carried on to the next generation. The three operations of DE are repeated until the desired misfit tolerance or the maximum iterations is reached.

2) Downhill Simplex: DHS is a local optimization algorithm that has the advantage of moving down the local gradient without evaluating the derivatives of the objective function [11]. To search for a better fit in an M-dimensional parameter space, DHS starts with a simplex of $M + 1$ model vectors, works its way towards the minimum misfit (downhill) through a series of steps such as reflection, reflection and expansion, contraction, and multiple contractions.

The reflection, expansion, and contraction are repeated until the desired maximum iterations or the relative error tolerance δ is reached. The relative error is designed in a sense of finding the smallest gradient between the highest misfit E_H and the lowest misfit E_L of the simplex to ensure DHS reaches the actual minimum

$$\frac{E_H - E_L}{0.5(E_H + E_L)} < \delta. \tag{4}$$

3) Outline of ASDE Algorithm: DE is recognized as one of the best evolution algorithms for optimizing real-valued functions, partly because of its faster convergence speed [12]. Faster convergence might lead to higher probability of being trapped in local minima. Since the fast convergence speed of DE is the result of a fast descent of the population diversity, one can increase the population size to reduce this drawback. However, the computation time increases with population size. The low efficiency is especially severe if most of the computation time is spent on forward modeling, as is often the case in geoacoustic inversions.

To improve the search efficiency, DHS is embedded into the DE algorithm whenever there is a better solution after each generation. This allows us to take the advantages of the DHS algorithm's simplicity and efficiency in finding the local minimum, and make use of the ability of the DE algorithm of moving out of the local minimum at the same time. Moreover, DHS's method of evaluating the algorithm convergence as shown in (4) can be adopted. This is important since for a real-world optimization problem, the minimum value of the objective function is not always known. Therefore, it is not practical to set an absolute

misfit tolerance for the algorithm convergence as the DE algorithm requires.

The flow chart of ASDE is shown in Fig. 7. The initial population of an ASDE run is chosen randomly in the sense of covering the whole parameter space uniformly. In the DE part of ASDE, the randomness is also required to ensure the uniform probability distribution of the model parameters. In the DHS part of ASDE, a perturbation term is added to the original simplex to introduce randomness to the DHS for high efficiency [13]. The perturbation size is determined adaptively according to the average of the model changes of the accepted models. An optional step is the quenching procedure after the maximum DE iteration is reached, which is essentially an enforced multi-iteration DHS for the final effort of finding the closest minimum [13].

4) Performance Comparison of ASDE Algorithm: Many other optimization techniques have been applied in geoacoustic inversion, such as simulated annealing [14], genetic algorithms [15], hybrids such as adaptive simplex simulated annealing (ASSA) [13], and more recently, Tabu [16] and ant colony optimization [17]. A comparison of the performance of DE, ASDE, and ASSA [13] is carried out by applying them to three multimodal optimization problems.

1) Multimodal function [18]: The number of parameters to be inverted is 6. This is a function that has multiple local minima

$$
\begin{aligned}
E(x_1, & x_2, x_3, x_4, x_5, x_6) \\
= {}& 4.8 + x_1^2 + 5x_2^2 + 0.1x_3^2 + 0.05x_4^2 + x_5^2 + x_6^2 \\
& - 0.3\cos 4\pi(x_1 - x_2) - 1.4\cos 4\pi(x_1 + x_2) \\
& - 0.5\cos 10\pi(0.05x_4 - 0.1x_3) \\
& - 1.0\cos 10\pi(0.05x_4 + 0.1x_3) \\
& - 0.25\cos 5\pi(x_5 - x_6) - 1.35\cos 5\pi(x_5 + x_6).
\end{aligned}
\tag{5}
$$

2) Rosenbrock's function [19]: The number of parameters to be inverted is 10. This function presents a difficult challenge to reach the global minimum

$$
E(x) = \sum_{i=2}^{10} 100\left(x_i - x_{i-1}^2\right)^2 + (1 - x_{i-1})^2,
$$
$$
i = 1, 2, \ldots 10. \tag{6}
$$

3) A standard matched-field geoacoustic inversion problem. The data used is case "so-1km-lfa" that was generated for the 1997 geoacoustic inversion workshop [20]. The problem is a single sediment layer over a half-space plus uncertainties in the source range and depth. The number of parameters to be inverted is 8.

The comparison is presented in terms of the final misfit and the number of model evaluations in Table I. The values in Table I are obtained from the best inversion results of each optimization algorithm. In terms of the quality of the solution (how close the estimates are to the true solutions), all of the optimization algorithms have almost perfect matches to the true values for Problem 1, while the ASDE solutions are better for the other two problems. In terms of the speed of
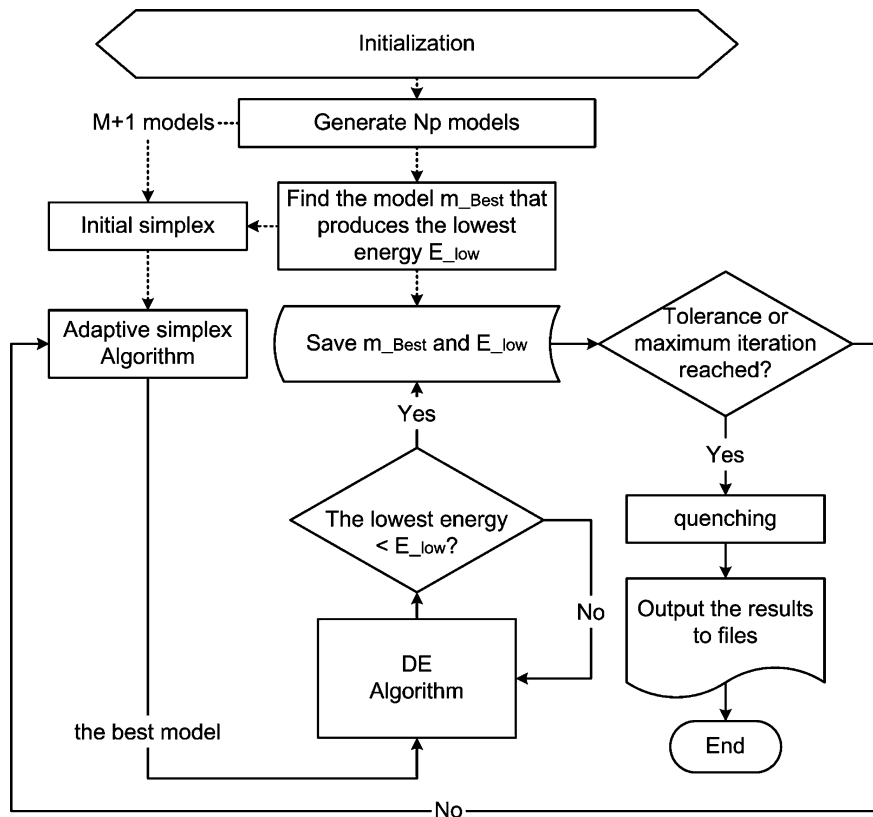
Fig. 7. Flow chart of ASDE algorithm. The dotted arrows indicate the initial procedures.

TABLE I
COMPARISON OF ASDE AND ASSA ALGORITHMS

Problem	Algorithm	Number of model evaluation	Misfit
	ASDE	19153	1.80×10^{-7}
1	ASSA	31336	1.79×10^{-7}
	DE	23221	1.79×10^{-7}
	ASDE	68904	5.94×10^{-8}
2	ASSA	200258	1.43×10^{-7}
	DE	224301	6.22×10^{-8}
	ASDE	23805	1.08×10^{-4}
3	ASSA	35301	1.05×10^{-4}
	DE	25241	1.07×10^{-4}

finding the global minimum, ASDE is more efficient for all three problems, and has obvious advantage in solving Rosenbrock's problem.

The ASDE algorithm is introduced here to show one of our efforts on developing highly efficient and simple optimization algorithms for geoacoustic inversion. It is worth mentioning that one should choose the searching algorithm appropriately [15] for a particular inversion problem. Although Table I indicates a better performance (in terms of efficiency) for ASDE in the chosen problem set, we will not conclude that ASDE is a better optimization algorithm overall. Comparing with ASSA and DE, ASDE has more control parameters and consequently may be less flexible in application. Complexity in determining the control parameters might lead to instability of the algorithm.

E. Acoustic Forward Model

Since the bathymetry between the source and the VLA was almost flat with only 0.6-m variation over 230-m range, range independence is assumed in the analysis. A range-independent ray tracing model was developed. The media between the source and the receiver are modeled as multiple homogenous horizontal layers. The acoustic properties such as sound speed and density within each layer are homogenous. The model searches for the ray parameters for the eigenrays connecting the source and the receiver within a range tolerance. The ray parameter for the ith hydrophone p_i is constant in each layer

$$p_i = \cos(\varphi_{ij})/c_j \qquad (7)$$

where φ_{ij} is the grazing angle at the jth layer for the ith hydrophone and c_j is the sound speed in layer j. The range tolerance used in this study is 0.5 cm. The ray parameters are stored when the inversion algorithm converges. Hence, the ray launching angles, receiving angles, and the travel length in each layer can be obtained for further study. It should be mentioned that this simple ray tracing program does not have the ability to deal with beam displacement at grazing angles less than the critical angle.

The performance of the ray tracing program in predicting travel times of the arrivals was examined for simulated data generated by the normal mode acoustic model ORCA [21]. First, time series were generated for hydrophones 8–14 by ORCA. A single-sediment-layer over half-space geoacoustic model was used. The parameters for the sea bottom were as follows: sediment sound speed 1550 m/s, sediment layer thickness 10 m, and

the basement sound speed 1700 m/s. The SSP used was derived from CTD37. The experimental geometries were as follows: the range 230 m, water depth 79.0 m, source depth 65 m, and array tilt 0°. Next, the travel-time differences between the arrivals reflected by the sediment and basement interface and the BR paths were picked and then put in the inversion. The search bounds for the sediment sound speed were [1510 1600] m/s, and for the layer thickness, [5 15] m. The estimated sediment sound speed was 1549.5 m/s and the layer thickness was 9.96 m, which were considered to be a good match.

F. Parameterization of the Geoacoustic Model

The geoacoustic parameterization is based on the resolvable sub-bottom reflections in the data, which essentially depends on the time resolution of the signal transmitted and the strength of the reflections from the sediment fine structure. The signal time resolution δT, which is defined as $\delta T = 0.886/B$ [22], determines the ability of separating two adjacent signals in the time domain. B is the signal bandwidth, here 3 kHz. The time resolution of the chirp signal discussed in this study is 0.3 ms, which means the signal has the ability to identify the arrivals whose travel path length difference is approximately 0.5 m for a sound speed of 1600 m/s.

The acoustic impedance contrast at the interface of two layers determines the inherent strength of the reflection. Several factors may affect the identification of the sub-bottom reflections from the signal strength information. For example, the reflected signals will be weakened by the sediment attenuation and scattering processes within the layers. The reflected signals that finally reach the hydrophones may be contaminated with noise.

It is evident in Fig. 4(b)–(f) that there exists at least one sub-bottom reflection in the signals for the 25–65-m sources. The fact that the signals are received by more than three hydrophones in each panel in Fig. 4 helps identifying the sediment layer reflections. Additional weak signals are also found within the sub-bottom reflection time region in some of the data, but it is difficult to confirm these layer reflections because they are isolated signals with very low signal-to-noise ratio (SNR). A simple method is applied to the data to amplify the signals to find more possible sub-bottom reflections that are too weak to show. Specifically, an after-the-fact time-varying gain (TVG) is designed according to the SNR

$$\text{TVG}(T_i) = \exp[(S(T_i) - \bar{S})/\sigma_{\text{amp}}] \quad (8)$$

where $S(T_i)$ is the averaged envelope of the received signal, T_i is the discrete time, $\bar{S}$ is the average noise level of the time series, and σ_{amp} determines the degree of the nonlinearity of the gain. $\text{TVG}(T_i)$ is then applied to $S(T_i)$ to obtain the enhanced time series $Z(T_i) = \text{TVG}(T_i) \times S(T_i)$.

Appropriate values of σ_{amp} are needed when generating the TVG series. σ_{amp} should be set to adequate values so that sufficient TVG is applied to the signal, and at the same time, the amplified waveform is not severely distorted. Normally σ_{amp} is determined according to the amplitude range of the signal to be amplified. A rule of thumb is that σ_{amp} is the -3 dB point of the maximum amplitude in the signal section to be enhanced

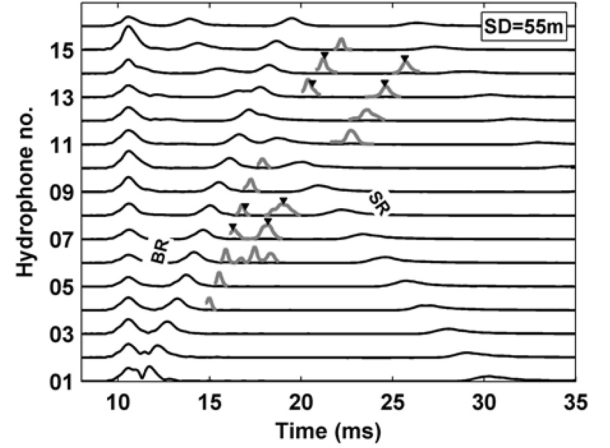$$\sigma_{\text{amp}} = \max\{S(T_i)\}/\sqrt{2}. \quad (9)$$

Fig. 8. Enhanced sub-bottom reflections (light thick curves) for 55-m source. The data clearly show two layers' reflections in the sediment. The black triangles are the travel-time prediction with inverted sediment parameters.

After applying TVG on the received time series, reflections from a layer above the strong reflector in Fig. 4 are visible; see Fig. 8. Since $\exp[\bullet]$ is a nonlinear function, and the amplitude of the waterborne arrivals are much greater than the subbottom reflections, we chose different σ_{amp} values for different sections of the time series signal when generating the TVG series.

Two geoacoustic models were adopted in the inversion. The first is a single sediment layer over a half-space, because reflections from one strong sediment reflector are evident in the data for 25–65-m sources; see Fig. 4. The second is two sediment layers over a half-space, since this model is supported by the enhanced time series. In spite of the very weak reflections from the additional layer, the two-sediment-layer model is tested to investigate the ability of resolving multiple layers by the inversion approach discussed here.

Since there is no information from the received signals that implies the sediment sound speed has positive or negative gradient, or other profiles, it is reasonable to assume that the sound speed is homogeneous within the layers. Hence, the averaged sound speed of the sediment, along with the sediment layer thickness, is inverted in the study.

G. Parameterization of the Oceanic Environment

To mitigate the impact of the ocean SSP variation on the travel-time geoacoustic inversion, a range-independent ocean SSP is inverted along with the experimental geometries before the inversion of the sediment properties. The ocean SSP is parameterized in terms of empirical orthogonal functions (EOFs) [23] and the inversion searches for the coefficients of the EOFs to construct an SSP that generates a better match to the measured data [24]–[27]. Apart from CTD36 and CTD37, the eight SSPs that are within 5 km of MPL-VLA1 on JD239 were used in the EOF analysis; see Fig. 9. Since the top and bottom of CTD36 and CTD37 are almost identical, only the middle part of the SSP, i.e., from 23 to 60 m, is used [26], [27]. The upper and lower portions are kept at the average values of CTD36 and CTD37 at those depths. By doing so, the search bounds of the SSP are further constrained, and the number of EOFs to be inverted is reduced.
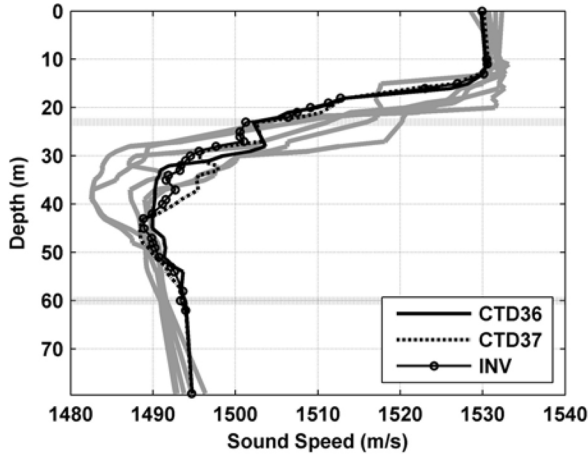
Fig. 9. CTD casts that are used in EOFs analysis. The SSP portion between the two horizontal dotted lines is the part to be inverted. The line with circles is the inverted SSP for the 25-m source.

Let $\mathbf{S}_L^K(N_Z)$ be the reconstructed residual SSP with L EOFs for the Kth SSP in the observation SSP set $\mathbf{S}(N_Z, N_S)$ (see the Appendix)

$$\mathbf{S}_L^K(N_Z) = \sum_{j=1}^{L} w_j^K v_j. \tag{10}$$

The degree of accuracy μ is defined as the energy ratio of $\mathbf{S}_L^K(N_Z)$ and the residual SSP $\mathbf{S}_r(N_Z, K)$

$$\mu = \sum_{p=1}^{N_Z} \left[\mathbf{S}_L^K(p)\right]^2 \Big/ \sum_{p=1}^{N_Z} [\mathbf{S}_r(p, K)]^2. \tag{11}$$

While inverting for the SSP, the number L of EOF coefficients to be inverted is found by examining the number of EOF coefficients needed to reconstruct an individual SSP to a prescribed accuracy μ (here 90%). L takes the maximum value of the number used to reconstruct every SSP in the observation set $\mathbf{S}(N_Z, N_S)$. This number reflects the difference of one individual SSP from the mean SSP $\bar{\mathbf{S}}(N_Z)$. If the effective SSP that is suitable for the propagation problem is greatly different from the mean SSP, it is expected that more EOFs are required. It should be noticed that this number is not necessarily the same as the number of the most significant eigenvalues in $\mathbf{\Lambda}_{\mathrm{EOF}}$.

The search bounds for each EOF coefficient are found by examining the values in the coefficient matrix $\mathbf{W}(N_J, N_Z)$

$$\mathbf{W}(N_J, N_S) = \mathbf{V}_{\mathrm{EOF}}^{\mathbf{T}} \cdot \mathbf{S}_r(N_Z, N_S). \tag{12}$$

Specifically, the following steps are taken to ensure sufficiently large bounds are used in the inversion: 1) find the maximum absolute value in each row of $\mathbf{W}(N_J, N_Z)$, where one row corresponds to one mode; 2) expand this value to about 5% and round the expanded value into the closest integer that has greater absolute value; 3) reflect this value to the other direction with respect to 0; and 4) collect the values in steps 2) and 3) to form the search bounds of that coefficient. For example, if the jth mode's coefficient $w_{j,k} \in [-15, 0.5]$, where $k = 1, \ldots, Ns$, then the final search bounds for the jth mode's coefficient are set to $[-16, 16]$.

TABLE II
INVERSION OF THE EXPERIMENTAL GEOMETRY

Parameter	Search bounds		Estimated value
	Lower	Upper	
Water depth (m)	78	81	79.2
Range (m)	220	240	233.4
Source depth (m)	60	70	64.6
Array tilt (°)	-6	6	0.8

TABLE III
SUMMARY OF BOTTOM PROPERTY ESTIMATES

Source depth (m)	Sound speed (m/s)	Layer thickness (m)	TWT (ms)
25	1609	21.5	26.7
35	1597	20.6	25.8
45	1600	22.3	27.9
55	1601	22.3	27.9
65	1584	20.4	25.8

IV. INVERSION RESULTS

This section presents the results of travel-time geoacoustic inversion of the MF chirps, and the comparison of the results with other experiments done in the vicinity.

A. The Geoacoustic Inversion Results

The control parameters of ASDE used for all of the inversion processes were set to the same values. The population size was 20 times the number of the parameters to be inverted, the mutation factor was 0.8, the crossover factor was 0.8, and the perturbation number in the DHS was 5.

1) Experimental Geometry: The experimental geometry was first examined in the inversion. In this step, the data were from the 65-m transmission and ocean SSP CTD37 that was measured immediately after the source transmissions at this depth. The search bounds and the results are listed in Table II.

2) Water-Column SSP: Four EOF coefficients were inverted for the reconstruction of the ocean SSP for further analysis of the data for 25–55-m sources. Data from the 25-m transmission are chosen to demonstrate the ocean SSP inversion result since the travel-time information was affected the most. The inverted SSP for the 25-m source is shown in Fig. 9, and the corresponding travel-time prediction is shown as black triangles in Fig. 6. It is seen that the modeled travel times for the inverted ocean SSP match the measured SR and BR arrival times at the hydrophones located under the thermocline very well, but are less accurate as the hydrophone depth decreases. Although the predicted travel times still have errors in the travel-time prediction, the results have been greatly improved compared with the predictions using CTD36 and CTD37. The maximum error between the modeled and measured travel time is 0.47 ms for the inverted SSP, which is much less than the maximum error of 2.1 ms for the measured SSPs in Fig. 6.

3) Sub-Bottom Sound Speed and Layer Thickness: A single-sediment-layer over half-space geoacoustic model was assumed first in the inversions of the data from 25- to 65-m source transmissions. The search bounds were 1550–1700 m/s for the sound speed and 5–30 m for the layer thickness. The estimates are summarized in Table III in terms of sediment sound speed, layer thickness, and derived two-way travel times (TWT).

TABLE IV
SUMMARY OF BOTTOM PROPERTY ESTIMATES FOR
TWO-SEDIMENT-LAYER MODEL

	Source depth = 55m			Source depth = 65m		
	Sound speed (m/s)	Layer thickness (m)	TWT (ms)	Sound speed (m/s)	Layer thickness (m)	TWT (ms)
Layer I	1581	11.9	15.1	1584	14.5	18.3
Layer II	1602	9.1	11.4	1611	8.4	10.4
Total	1592	21.0	26.5	1598	22.9	28.7

TABLE V
COMPARISON OF THE SEA BOTTOM PROPERTY ESTIMATES

Ref.	Frequency (kHz)	Method	Sound speed (m/s)	Layer thickness (m)
[23]	0.05 – 0.6	Transmission loss	1560 1610 1847	5 10 20
[24]	0.5-5.0	Arrival structure of wide angle time series	1594	19
[26]	2.0-11.0	*In situ* probe	1615±9 1598±11	0-3
[28]	1.0-20.0	Bottom loss and travel time	1680 1630±20	0.20 22±1
[19]	0.05-0.7	Matched field Inversion	1599	24
[20]	0.05-0.5	Matched field Inversion	1605	21

For the 55- and 65-m sources, there is evidence of reflections from more than one layer in the enhanced time series. The sub-bottom reflections are more complicated for the 65-m source. A two-sediment-layer over half-space model was then attempted in the analysis. The inversion compares only the travel-time differences of the hydrophones' signals that contained reflections from the two sub-bottom layers simultaneously. The estimates for the two sediment layers are listed in Table IV. The travel-time prediction from the two sediment layers for the 55-m source is shown in Fig. 8 as black triangles. The inversion results from the two-sediment-layer over half-space model are consistent with those from the single-sediment-layer over half-space model, in terms of the average sound speed in the sediment and the total thickness of sediment layer.

B. Comparison With the Work Done in the Vicinity

Many geoacoustic inversion studies have been done on the New Jersey continental shelf previously [28]–[31]. Most recently, a concentrated effort on the seabed characterization of the SW06 site was presented in a special issue of the Express Letters of the *Journal of the Acoustical Society of America* on SW06 [25]–[27], [32]–[37]. The TWTs from the chirp seismic reflection data between the source and the VLA [6] are plotted in Fig. 10.

The previous works that were done near the Atlantic Margin Coring Project (AMCOR) 6010 borehole [38], and the recent works near the experimental site are summarized in Table V. Overall, the sound speed obtained in this study is consistent with the *in situ* measurement [32]. The combination of sound speed
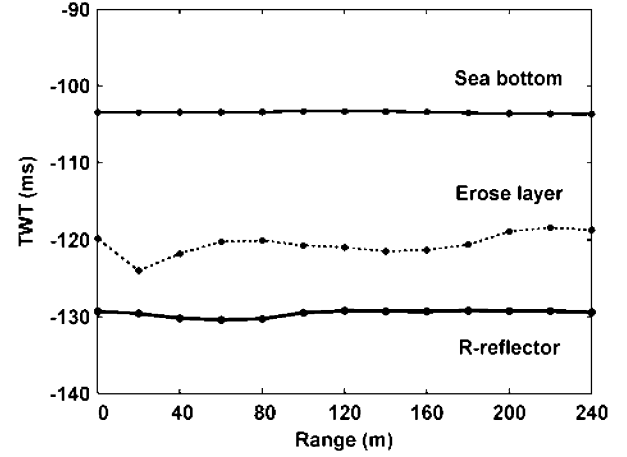

Fig. 10. Chirp seismic reflection data [6] between the source and the MPL-VLA1 obtained during SW06.

and sediment layer thickness also matches the chirp seismic reflection data very well in terms of TWT (26.1 ± 0.5 ms) from the seafloor down to the "R"-reflector [3], [6]. The estimates of the sound speed and layer thickness are consistent with the results from matched-field inversions of long-range data along the same radial track from the VLA [25], [26], and also consistent with the estimates that were previously done in the vicinity [29], [30].

V. SUMMARY

The experimental geometry using a VLA and a depth-varying source at short range provides a simple and effective method for wide angular coverage of reflections from the ocean bottom.

The hybrid optimization algorithm ASDE was efficient in the travel-time geoacoustic inversion of MF chirps collected on the New Jersey Continental Shelf. The effects of time-varying ocean environment on the travel times of the acoustic arrivals were mitigated by estimating the effective water-column SSPs before the geoacoustic inversion. The experimental geometry was also inverted before the geoacoustic inversion. The estimates of sediment SSP and the layer thickness are consistent with results from other works done in the vicinity.

APPENDIX
EOF REPRESENTATION OF THE OCEAN SSP

The ocean SSP observations $\mathbf{S}(N_Z, N_S)$ are first expressed in terms of the sum of the average of SSP $\bar{\mathbf{S}}(N_Z)$ and the residual SSPs $\mathbf{S_r}(N_Z, N_S)$

$$\mathbf{S}(N_Z, N_S) = \bar{\mathbf{S}}(N_Z) + \mathbf{S_r}(N_Z, N_S) \qquad (13)$$

where N_z is the number of SSP data points, and N_s is the number of SSP used. $\mathbf{S_r}(N_Z, N_S)$ is obtained by taking the differences between $\mathbf{S}(N_Z, N_S)$ and $\bar{\mathbf{S}}(N_Z)$. Next, $\mathbf{S_r}(N_Z, N_S)$ is expressed as a linear combination of a set of orthogonal functions, or an equivalent set of orthonormal functions [23], [24], and (13) is rewritten as follows:

$$\mathbf{S}(N_Z, N_S) = \bar{\mathbf{S}}(N_Z) + \mathbf{V}_{\text{EOF}} \cdot \left(\mathbf{V}_{\text{EOF}}^{\mathbf{T}} \cdot \mathbf{S}_r(N_Z, N_S)\right) \quad (14)$$

in which the superscript "$\mathbf{T}$" is the transpose operator. The orthonormal vector set $\mathbf{V}_{\text{EOF}}$ is obtained by finding the eigenvectors of the SSP residual covariance matrix $\mathbf{R}$

$$\mathbf{R} = E\left[\mathbf{S_r S_r^T}\right] = \mathbf{V}_{\text{EOF}}\mathbf{\Lambda}_{\text{EOF}}\mathbf{V}_{\text{EOF}}^{\mathbf{T}} \tag{15}$$

where $E[\cdot]$ is the expectation. $\mathbf{V}_{\text{EOF}}$ is an $N_Z \times N_J$ matrix, where N_J is the number of the significant eigenvectors. N_J takes the value of N_Z or N_S, whichever is less. Each eigenvector represents one mode of the SSP variations in depth. The coefficient of each eigenvector is found by projecting $\mathbf{V}_{\text{EOF}}^{\mathbf{T}}$ on $\mathbf{S_r}(N_Z, N_S)$

$$w_j^K = \left[\mathbf{S_r}(N_Z, K)\right]^{\mathbf{T}} v_j \tag{16}$$

where $j = 1, \ldots N_J, K = 1, \ldots N_S$, and v_j is the jth eigenvector of $\mathbf{V}_{\text{EOF}}$.

ACKNOWLEDGMENT

REFERENCES

[1] D. J. Tang, J. Moum, J. Lynch, P. Abbot, R. Chapman, P. Dahl, T. Duda, G. Gawarkiewicz, S. Glenn, J. Goff, H. Graber, J. Kemp, A. Maffei, J. Nash, and A. Newhall, "Shallow Water '06—A joint acoustic propagation/nonlinear internal wave physics experiment," *Oceanography*, vol. 20, no. 4, pp. 156–167, 2007.

[2] C. W. Holland and J. Osler, "High resolution geoacoustic inversion in shallow water: A joint time and frequency domain technique," *J. Acoust. Soc. Amer.*, vol. 107, pp. 1263–1279, 2000.

[3] J. A. Goff, B. J. Kraft, L. A. Mayer, S. G. Schock, C. K. Sommerfield, H. C. Olson, S. P. S. Gulick, and S. Nordfjord, "Seabed characterization on the New Jersey middle and outer shelf: Correlatability and spatial variability of seafloor sediment properties," *Mar. Geology*, vol. 209, pp. 147–172, 2004.

[4] T. A. Davies, J. A. Austin Jr., M. B. Lagoe, and D. Milliman, "Late quaternary sedimentation off New Jersey: New results using 3-D seismic profiles and cores," *Mar. Geology*, vol. 108, pp. 323–343, 1992.

[5] A. Turgut, D. Lavoie, D. J. Walter, and W. B. Sawyer, "Measurements of bottom variability during SWAT New Jersey Shelf Experiments," in *Impact of Littoral Environmental Variability on Acoustic Predictions and Sonar Performance*. Norwell, MA: Kluwer, 2002, pp. 91–98.

[6] J. A. Goff and J. A. Austin, Jr., "Seismic and bathymetric evidence for four different episodes of iceberg scouring on the New Jersey outer shelf: Possible correlation to Heinrich events," *Mar. Geology*, vol. 266, pp. 244–254, 2009.

[7] M. B. Porter and Y.-C. Liu, "Finite element ray tracing," in *Theoretical and Computational Acoustics*, D. Lee and M. H. Schultz, Eds. Singapore: World Scientific, 1994, vol. 2, pp. 947–953.

[8] R. Storn and K. Price, "Differential evolution—A simple and efficient heuristic for global optimization over continuous spaces," *J. Global Optim.*, vol. 11, no. 4, pp. 341–359, 1997.

[9] M. Snellen, D. G. Simons, and C. van Moll, "Application of differential evolution as an optimisation method for geoacoustic inversion," in *Proc. 7th Eur. Conf. Underwater Acoust.*, 2004, pp. 721–726.

[10] M. Snellen and D. G. Simons, "An assessment of the performance of global optimization methods for geo-acoustic inversion," *J. Comput. Acoust.*, vol. 16, pp. 199–223, 2008.

[11] W. H. Press, S. A. Teukolsky, W. T. Vetterling, and B. P. Flannery, *Numerical Recipes in Fortran*, 2nd ed. Cambridge, U.K.: Cambridge Univ. Press, 1992, pp. 402–406.

[12] H. Bersini, M. Dorigo, S. Langerman, G. Seront, and L. Gambardella, "Results of the first international contest on evolutionary optimization (1st ICEO)," in *Proc. IEEE Int. Conf. Evol. Comput.*, 1996, pp. 611–615.

[13] S. E. Dosso, M. J. Wilmut, and A. S. Lapinski, "An adaptive-hybrid algorithm for geoacoustic inversion," *IEEE J. Ocean. Eng.*, vol. 26, no. 3, pp. 324–336, Jul. 2001.

[14] C. E. Lindsay and N. R. Chapman, "Matched field inversion for geoacoustic model parameters using adaptive simulated annealing," *IEEE J. Ocean. Eng.*, vol. 18, no. 3, pp. 224–231, Jul. 1993.

[15] P. Gerstoft, "Inversion of acoustic data using a combination of genetic algorithms and the Gaussian-Newton approach," *J. Acoust. Soc. Amer.*, vol. 97, pp. 2181–2190, 1995.

[16] Z.-H. Michalopoulou and U. Ghosh-Dastidar, "Tabu for matched-field source localization and geoacoustic inversion," *J. Acoust. Soc. Amer.*, vol. 115, pp. 135–145, 2004.

[17] V. Leijen and J.-P. Herman, "Geoacoustic inversion with ant colony optimisation," in *Proc. 8th Eur. Conf. Underwater Acoust.*, 2006, pp. 515–520.

[18] M. Musil, M. J. Wilmut, and N. R. Chapman, "A hybrid simplex genetic algorithm for estimating geoacoustic parameters using matched-field inversion," *IEEE J. Ocean. Eng.*, vol. 24, no. 3, pp. 358–369, Jul. 1999.

[19] A. Dolan, "A general GA toolkit implemented in Java, for experimenting with genetic algorithms and handling optimization problems," 2003 [Online]. Available: http://www.aridolan.com/ofiles/ga/gaa/Rosenbrock.aspx

[20] A. Tolstoy, N. R. Chapman, and G. E. Brooke, "Workshop '97: Benchmarking for geoacoustic inversion in shallow water," *J. Comput. Acoust.*, vol. 6, pp. 1–28, 1998.

[21] E. K. Westwood, C. T. Tindle, and N. R. Chapman, "A normal mode model for acousto-elastic ocean environments," *J. Acoust. Soc. Amer.*, vol. 100, pp. 3631–3645, 1996.

[22] X. Lurton, *An Introduction to Underwater Acoustics—Principles and Applications*. New York: Springer-Verlag, 2004, pp. 200–.

[23] L. R. LeBlanc and F. H. Middleton, "An underwater acoustic sound velocity data model," *J. Acoust. Soc. Amer.*, vol. 67, pp. 2055–2062, 1980.

[24] P. Gerstoft and D. F. Gingras, "Parameter estimation using multifrequency range-dependent acoustic data in shallow water," *J. Acoust. Soc. Amer.*, vol. 99, pp. 2839–2850, 1996.

[25] C.-F. Huang, P. Gerstoft, and W. S. Hodgkiss, "Effect of ocean sound speed uncertainty on matched-field geoacoustic inversion," *J. Acoust. Soc. Amer.*, vol. 123, pp. EL162–EL168, 2008.

[26] Y.-M. Jiang and N. R. Chapman, "Bayesian geoacoustic inversion in a dynamic shallow water environment," *J. Acoust. Soc. Amer.*, vol. 123, pp. EL155–EL161, 2008.

[27] Y.-M. Jiang, N. R. Chapman, and P. Gerstoft, "Short range geoacoustic inversion with vertical line array," *J. Acoust. Soc. Amer.*, vol. 124, no. 3, pt. 2 of 2, pp. EL135–EL140, 2008.

[28] B. J. Kraft, I. Overeem, C. W. Holland, L. F. Pratson, J. P. M. Syvitski, and L. A. Mayer, "Stratigraphic model predictions of geoacoustic properties," *IEEE J. Ocean. Eng.*, vol. 31, no. 2, pp. 266–283, Apr. 2006.

[29] W. M. Carey, J. Doutt, R. B. Evans, and L. M. Dillman, "Shallow-water sound transmission measurements on the New Jersey continental shelf," *IEEE J. Ocean. Eng.*, vol. 20, no. 4, pp. 321–336, Oct. 1995.

[30] C. W. Holland, J. Dettmer, and S. E. Dosso, "A technique for measuring *in situ* compressional wave speed dispersion in marine sediments," *IEEE J. Ocean. Eng.*, vol. 30, no. 4, pp. 748–763, Oct. 2005.

[31] Y.-M. Jiang, N. R. Chapman, and M. Badiey, "Quantifying the uncertainty of geoacoustic model parameters for the New Jersey shelf by inverting air gun data," *J. Acoust. Soc. Amer.*, vol. 121, pp. 1879–1895, 2007.

[32] J. Yang, D. J. Tang, and K. L. Williams, "Direct measurement of in situ sediment sound speed at SW06," *J. Acoust. Soc. Amer.*, vol. 124, no. 3, pt. 2 of 2, pp. EL116–EL121, 2008.

[33] A. Turgut and T. Yamamoto, "*In situ* measurements of velocity dispersion and attenuation in New Jersey shelf sediments," *J. Acoust. Soc. Amer.*, vol. 124, no. 3, pt. 2 of 2, pp. EL122–EL127, 2008.

[34] J. W. Choi, P. H. Dahl, and J. A. Goff, "Observations of the R reflector and sediment interface reflection at the shallow water '06 central site," *J. Acoust. Soc. Amer.*, vol. 124, pp. EL128–EL134, 2008.

[35] M. S. Ballard and K. M. Becker, "Geoacoustic inversion on the New Jersey margin," *J. Acoust. Soc. Amer.*, vol. 124, no. 3, pt. 2 of 2, pp. EL141–EL145, 2008.

[36] G. R. Potty, J. H. Miller, P. S. Wilson, J. F. Lynch, and A. Newhall, "Geoacoustic inversion using combustive sound source signals," *J. Acoust. Soc. Amer.*, vol. 124, no. 3, pt. Pt. 2 of 2, pp. EL146–EL150, 2008.

[37] D. P. Knobles, P. S. Wilson, J. A. Goff, and S. E. Cho, "Seabed acoustics of a sand ridge on the New Jersey continental shelf," *J. Acoust. Soc. Amer.*, vol. 124, no. 3, pt. 2 of 2, pp. EL151–EL156, 2008.

[38] J. C. Hathaway, C. W. Poag, P. C. Valentine, R. E. Miller, D. M. Schultz, F. T. Manhiem, F. A. Kohout, M. H. Bothner, and D. A. Sangrey, "U.S. geological survey core drilling on the Atlantic shelf," *Science*, vol. 206, pp. 515–527, 1976.

Yong-Min Jiang (M'04) received the B.Sc. degree in acoustics from Peking (Beijing) University, Beijing, China, in 1986 and the M.S. and Ph.D. degrees in underwater acoustic engineering from Harbin Engineering University, Harbin, China, in 1995 and 2001, respectively. Her M.S. thesis focused on characterization of underwater acoustic channels and her Ph.D. dissertation focused on modeling techniques of high-frequency backscattering from near field targets.

She was with Dalian Scientific Test and Control Technology Institute, Dalian, China, from 1986 to 2002, where she became a Senior Research Engineer in 1996 and a Research Professor in 2001. Her research interests were full/scaled underwater target backscattering feature extraction, modeling, measurement methodologies, and related signal processing. Her management positions included the Vice Chief Engineer of the Institute and the Director of the Underwater Target Backscattering Research Department. She has been a Research Associate Scientist in the Ocean Acoustic Group, University of Victoria, Victoria, BC, Canada, since 2002. Her current research interests are geoacoustic inversion, inversion algorithms, and underwater acoustic propagation modeling.

Dr. Jiang is a member of the Acoustical Society of America.

N. Ross Chapman (M'97–SM'03–F'10) received the Ph.D. degree in physics from the University of British Columbia, Vancouver, BC, Canada, in 1975.

He was the Group Leader of the Ocean Acoustics Group, Defence Research Establishment Pacific, Victoria, BC, Canada. In 1995, he was appointed Senior Chair in Ocean Acoustics, University of Victoria, Victoria, BC, Canada. His research interests include acoustic and seismoacoustic propagation modeling, and the development of inverse methods for localization and estimation of geoacoustic model parameters of the ocean bottom.

Dr. Chapman is a Fellow of the Acoustical Society of America.

Peter Gerstoft received the M.Sc. and the Ph.D. degrees in structural engineering from the Technical University of Denmark, Lyngby, Denmark, in 1983 and 1986, respectively.

From 1987 to 1992, he was employed at Ødegaard and Danneskiold-Samsøe, Copenhagen, Denmark, working on forward modeling and inversion for seismic exploration. From 1992 to 1997, he was a Senior Scientist at SACLANT Undersea Research Centre, La Spezia, Italy, where he developed the SAGA inversion code, which is used for ocean acoustic and electromagnetic signals. Since 1997, he has been with Marine Physics Laboratory, University of California, San Diego. His research interests include global optimization, modeling and inversion of acoustic, and elastic and electromagnetic signals.

Dr. Gerstoft is a Fellow of the Acoustical Society of America and an elected member of the International Union of Radio Science, Commission F.